ELASTIC GEOBAROMETRY METHODS: VALIDATION THROUGH SYNTHESIS AND CHARACTERIZATION OF HOST-INCLUSION PAIRS BY MEANS OF RAMAN SPECTROSCOPY

MATTIA BONAZZI
Dipartimento di Scienze della Terra e dell'Ambiente, Università degli Studi di Pavia, Via Ferrata 1, 27100 Pavia

INTRODUCTION

For the Earth sciences the determination of pressure conditions is fundamental to understand the formation of the rocks or their evolution. However, the conventional geobarometry based on the thermodynamics equilibrium of phase assemblages is challenged in subduction environments. An excellent way to determine the pressure conditions in High-Pressure (HP) and Ultra-High-Pressure (UHP) is to apply the elastic geobarometry method for the host-inclusion pairs. For example, in the HP conditions a common host-inclusion pairs is garnet with quartz inclusions. Elastic geobarometry is based on the difference of elastic proprieties between host and inclusion pairs to calculate the entrapment pressure of inclusions. The elastic proprieties of minerals are described by elastic tensor or equation of state. The entire method is based on concept that the quartz inclusion fully trapped in the garnet host exhibit a "residual" pressure different from external pressure. The residual pressure is related to entrapment conditions. This concept has been reported for the first time by Rosenfeld & Chase (1961) and in the last twenty years has been utilized extensively to interpreting the residual pressures of inclusions in diamonds (*e.g.*, Izraeli *et al*., 1999; Nestola *et al*., 2011; Howell *et al*., 2012). Even if this method has been already applied in natural rocks, an experimental validation is necessary because the exact P and T of entrapment are known in synthetic host-inclusions pairs. The determination of residual pressures on the recovered inclusions have been performed with Raman spectroscopy following different approaches.

In this thesis the main goals were: *i*) to synthesize one or more inclusion minerals trapped in monocrystalline cubic host with well-known elastic proprieties; *ii*) to demonstrate the validity of the numerous elastic geobarometry methods that are reported in literature (*e.g.*, Angel *et al.*, 2017; Murri *et al.*, 2018; Schmidt & Ziemann, 2000) through the synthesis of host inclusions system in laboratory.

In order to achieve these aims, we chose to carry out the syntheses following two approaches: *i*) solid-state synthesis that consists to use monocrystalline garnet rods as seed crystals to permit the epitaxial growth of new garnet (Ikesue & Aung, 2006) which will also trap inclusion phases mixed into the crystalline powder of the same compositions of seed. During the project after the preliminary results we decided to move on and change the type of powder from crystalline to non-crystalline. The advantage of solid-state synthesis is the fine control on the size and position of the inclusions and then permit us to measure the inclusions using X-ray single crystal diffraction and Raman Spectroscopy; *ii*) hydrothermal synthesis, which consists of an oxide mixture plus water at eclogitic conditions (*e.g.*, Thomas & Spear, 2018; Bonazzi *et al.*, 2019). From this starting material crystallized free single crystals of garnet with a lot of small quartz inclusions and other minerals, immersed in fluid. The advantage of this approach allowed us to measure several inclusions in different hosts obtained from the same experiment. From these syntheses we provided a statistical information on reliability of elastic measurements on inclusions.

SOLID-STATE SYNTHESIS

Experimental methods

The solid-state experiments were performed using HT Gas Mixing furnace (only YAG6 experiment) and piston cylinder end loaded apparatus for all other experiments.

We loaded a capsule with monocrystalline rods (ø 1.8 or 2.7 mm) together with crystalline or non-crystalline powder of the same material (Fig. 1a and 1b).

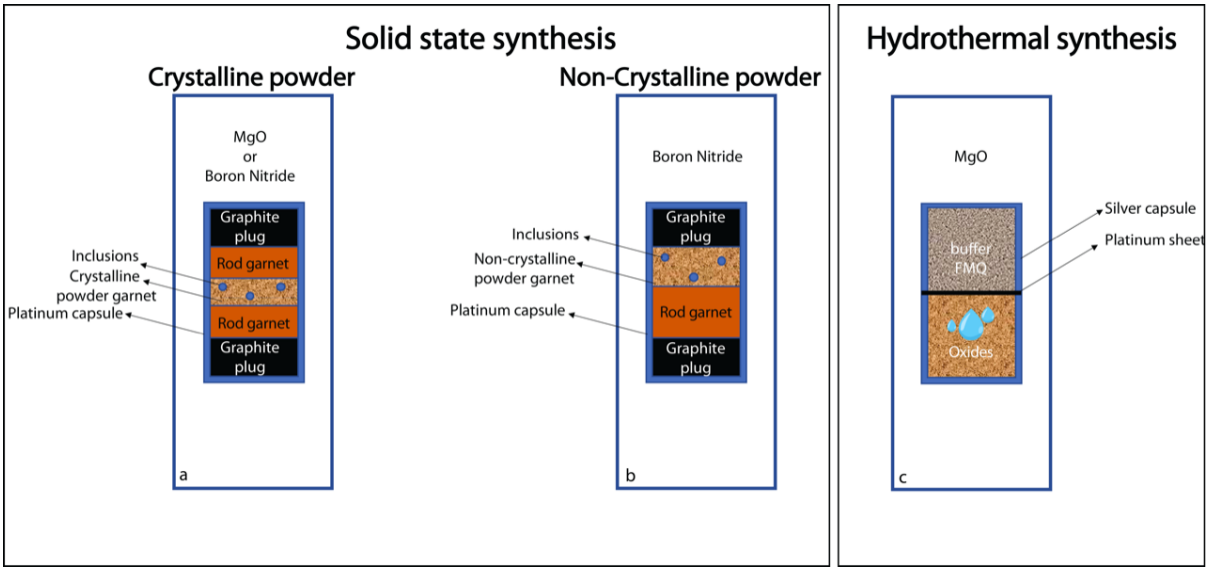

Fig. 1 - Sketch of starting material for solid-state experiments with crystalline powder (a), non-crystalline powder (b) and hydrothermal synthesis (c).

In the powder we inserted a different phase that should have been included during the host growth. At high P and T, the powder will grow as a single crystal following the crystallographic orientation of the rod (*e.g.*, in epitaxial conditions with respect to the rod surface). We used two different monocrystalline rods for solid-state experiments: yttrium aluminum garnet (YAG) and natural pyrope. From the cylinder we obtained rod of about 1 mm in thickness using a diamond circular saw. In addition, the rod surface, where the epitaxial growth occurred, were mirror polished (up to 1 µm). The crystalline powder was produced by comminution of YAG and natural pyrope rods and its grain size was < 200 µm. The non-crystalline powder of pyrope composition were prepared using two different methods: gels and glass.

All experiments were performed at constant high pressure (3 GPa) excluding YAG6 (at room P). However, the temperature of synthesis was dependent by the type of mineral phase mixed with the powder. For example, in the experiments with amorphous SiO_2 the temperature runs were limited at 1200°C and 1150°C to keep the synthesis in the α-quartz stability field.

The other phases mixed with powder to be trapped as inclusions were: *i*) for YAG experiments: Ruby, metallic Si, metallic Ti, diamond; *ii*) for natural pyrope experiments: diamond, amorphous SiO_2, synthetic cristobalite, natural quartz. Synthetic cristobalite were obtained through heat treatment starting by amorphous SiO_2.

As well, the choice of assembly and capsule was dependent by temperature and pressure conditions. The salt-pyrex assembly with graphite furnace was used for experiment under 1150°C, whereas for over temperatures the salt-pyrex assembly was replaced with talc-quartz assembly. The capsules were accommodated in MgO or boron nitrate (BN) rods; the boron nitride distribute more homogenously the stress to high temperature (Tingle, 1988). BN rods and powders were fired for 24 hours at 1100°C before the experimental run. Corundum disk was placed at the top of the MgO or BN rod to avoid contact between capsule and thermocouple, which could lead to the piercing of the capsule. For experiments we used gold or platinum capsule. The melting point of platinum is higher than gold (1768°C and 1064°C, respectively at environment pressure), thus Pt was used to high temperature. In these experiments it was important to avoid fracturing of the host because in that case the elastic geobarometry cannot be applied. For this reason, from YAG7 we followed Tingle (1988) protocol that used two

practical arrangements to avoid fracturing. First, we placed at the top and at the bottom of the capsule two graphite plugs because they are able to accommodate the stress release. Second, we performed a linear and slow ramp up and down for temperature and pressure that should avoid fracturing of the crystal (Tingle, 1988). Then, from experiment YAG7 (Table 1), we putted two graphite plugs at top and bottom of capsule and we applied pressuring and depressuring ramps to prevent cracking during the quenching of the experiments.

Table 1 - Summary of solid-state synthesis experiments.

	CAPSULE				STARTING MATERIALS				EXP CONDITIONS			RAMPS	
Exp name	**Ass**	**Mat**	**Ø** (cm)	**Graph plugs**	**Rod mat**	**N° rod**	**Powder**	**Incl**	**T** (°C)	**P** (GPa)	**t** (hours)	**Up**	**Down**
YAG3		Au	3	no	YAG	2	cryst YAG	ruby	1000	3	144	-	quench
YAG4	salt pyrex	Au	3	no	YAG YAG	2	cryst YAG	ruby	1200 growth 800 el reset	3	120	-	quench
YAG5		Au	3	no	YAG YAG	2	cryst YAG	ruby	1300 growth 800 el reset	3	96	-	quench
YAG6	-	Pt	3	no	YAG	2	cryst YAG	-	1700	room P	48	-	quench
YAG7	salt pyrex	Pt	3	no	YAG	2	cryst YAG	Si met	1300	3	30	YAG7	YAG7
YAG8		Pt	3	no	YAG	2	cryst YAG	Ti met	1300	3	24	YAG7	YAG7
YAG9		Pt	3	no	YAG	2	cryst YAG	Dia	1300	3	24	YAG7	YAG7
YAG10		Pt	3	no	YAG	2	cryst YAG	Dia	1300	3	24	YAG7	YAG7
YAG11		Pt	3	no	YAG	2	cryst YAG	Dia	1300	3	24	YAG7	YAG7
Py1	salt pyrex	Pt	2	yes	Py	2	cryst nat py	Dia	1300	3	16	YAG7	quench
Py2		Pt	2	yes	Py	2	cryst nat py	Dia	1300	3	12	YAG7	YAG7
Py3		Pt	2	yes	Py	2	cryst nat py	Dia	1300	3	23	YAG7	YAG7
Py4	talc Qz	Pt	3	yes	Py	2	cryst nat py	SiO_2 gels	1200	3	90	YAG7	PY4
Py5		Pt	3	yes	Py	1	cryst nat Py	SiO_2 gels	1200	3	44	YAG7	PY4
Py6		Pt	3	yes	Py	2	cryst nat Py	SiO_2 gels dehyd	1200	3	117	YAG7	PY4
Py7		Pt	3	yes	Py	1	cryst nat Py	SiO_2 gels dehyd	1200	3	138	YAG7	quench
Py8	salt pyrex	Pt	3	yes	Py	1	cryst nat Py	nat Qz	1150	3	67	YAG7	quench
Py9		Pt	3	yes	Py	1	cryst nat Py	Crs	1150	3	46	YAG7	quench
Py10	talc Qz	Pt	3	yes	Py	1	Py gel	Crs	1200	3	77	YAG7	quench
Py11		Pt	3	yes	Py	1	Py gel	Crs	1200	3	???	YAG7	quench

Mineral abbreviations are: Grahp-graphite, Qz-quartz, Dia-diamond, Py-pyrope, Crs-cristobalite. Word abbreviations are: Exp-experiements, Ass-assembly, Mat-materials, Ø-diameter, Incl-inclusion, T-temperature, P-pressure, t-time, cryst-crystalline, el reset-elastic resetting, met-mettalic, nat-natural, dehyd-dehydration.

Samples were first pressurized to P = 0.25 GPa, heated to T = 800°C and then pressurized and heated simultaneously up to 1 GPa and 1000°C. At this temperature, the sample were pressurized up to 3 GPa and in the final step only heated keeping constant pressure. Temperature rate was 50°C/minute until reaching the final value. From run conditions to room P and T, the experiments were depressurized approximately at a rate of about 80/100 MPa/min with a temperature cooling ramp in 2 steps from 1300/1200°C to 1000 (to 2.5 GPa) and from 1000 to 200°C (simultaneously to pressure) and final temperature.

Results and discussions

We performed 20 experiments using solid-state method to synthesize host-inclusion system (Table 1). These experiments explored the grains growth of single crystal during sintering process for synthetic garnet of yttrium and aluminum (YAG- $Y_3Al_5O_{12}$) and natural pyrope.

For the first solid state-experiments we used YAG as host because it has similar elastic proprieties of natural garnet (*e.g.*, Rezende, 2014); however, the growth rate of YAG is faster than natural garnet (Ikesue & Aung, 2006). The YAG6 was performed without other phases at close melting conditions (1700°C) and room pressure using gas mixing. In this experiment the role of temperature during sintering processes were observed.

Bonding occurred where the grains were in contact, but porosity was not decreased. Then the pressure was fundamental to obtain sintering of high quality. In the next experiments we ran the synthesis with pressure. In these experiments we mixed ruby crystals with crystalline YAG powder. The final result was a lot of YAG disk with thickness less than 0.3 mm. The presence of ruby inclusions was checked using X-ray diffraction, but we found no-inclusions. From YAG7 experiment we placed two plugs of graphite at top and at bottom inside the capsule (see Fig. 1a and 1b) to prevent the cracks (Tingle, 1988). In Experiments YAG7 and YAG8 we inserted metallic Si and metallic Ti mixed with YAG crystalline powder, respectively. The inclusions reached with host and Pt capsule. For this reason, to prevent the reaction of other phases with YAG, we inserted diamond inclusions. The diamond is well-known as no-reactive mineral. However, also the diamond reacted with YAG.

As consequence of YAG reactivity, we had to delineate a new strategy for host. We replaced YAG with Pyrope of Dora Maira locality (natural garnet). The Dora Maira garnet megablasts consist of pyrope (90-98 mol.%) and their composition are relative homogeneous in all crystals (*e.g.*, Chopin, 1984; Simon *et al*., 1997; Compagnoni & Hirajima, 2001). In the first experiments with pyrope, we mixed diamond with pyrope powder. The diamonds seemed fully trapped in garnet host. However, the garnet around the inclusions is polycrystalline and the diamond is transformed in cubic crystals of order graphite. Due to high speed of diamond-graphite transition at these P and T conditions, we replaced the diamond phases with SiO_2.

In the subsequent experiments, we synthetized pyrope crystalline powder with different type of SiO_2 phases (amorphous spherical SiO_2, irregular natural quartz and synthetic spherical cristobalite). The best result was obtained from sphere of cristobalite because it was not melted or fractured and during the synthesis cristobalite was turned into quartz. However, From EBSD analysis on solid-state experiments with crystalline powder we understood also that the sintering process improved significantly at higher temperature; therefore, the time to grow suitable sized grains was too long to have single crystals. At this point we replaced the crystalline powder with non-crystalline powders (gels and glasses) of pyrope because it is more reactive (Fig. 1b) and we mixed cristobalite with both gels and glasses non-crystalline powders. The result of experiment Py10 with gel powder was a heterogenous host where there were four minerals phases: pyrope, corundum, enstatite, and periclase. The experiment Py11, with glass of pyrope as powder, showed that there was a big crystal of quartz as host and the pyrope included in quartz. Probably the preparation of glass was not good because we didn't have a homogeneous glass in all parts and in the Py11 we used a Si-rich part. For both hosts, the planar fractures decreased using the graphite plugs at top and bottom of capsule.

HYDROTHERMAL SYNTHESIS

Experimental methods

We measured quartz inclusions in almandine garnet resulted from the hydrothermal synthesis in the end-loaded piston cylinder apparatus at Syracuse University Laboratory. The experiments were performed at 3 GPa and 775°C (Fig. 2a and b; Alm-1) and 2.5 GPa and 800°C (Alm-2), *i.e.*, typical eclogitic conditions, with run times between 72 and 96 hours.

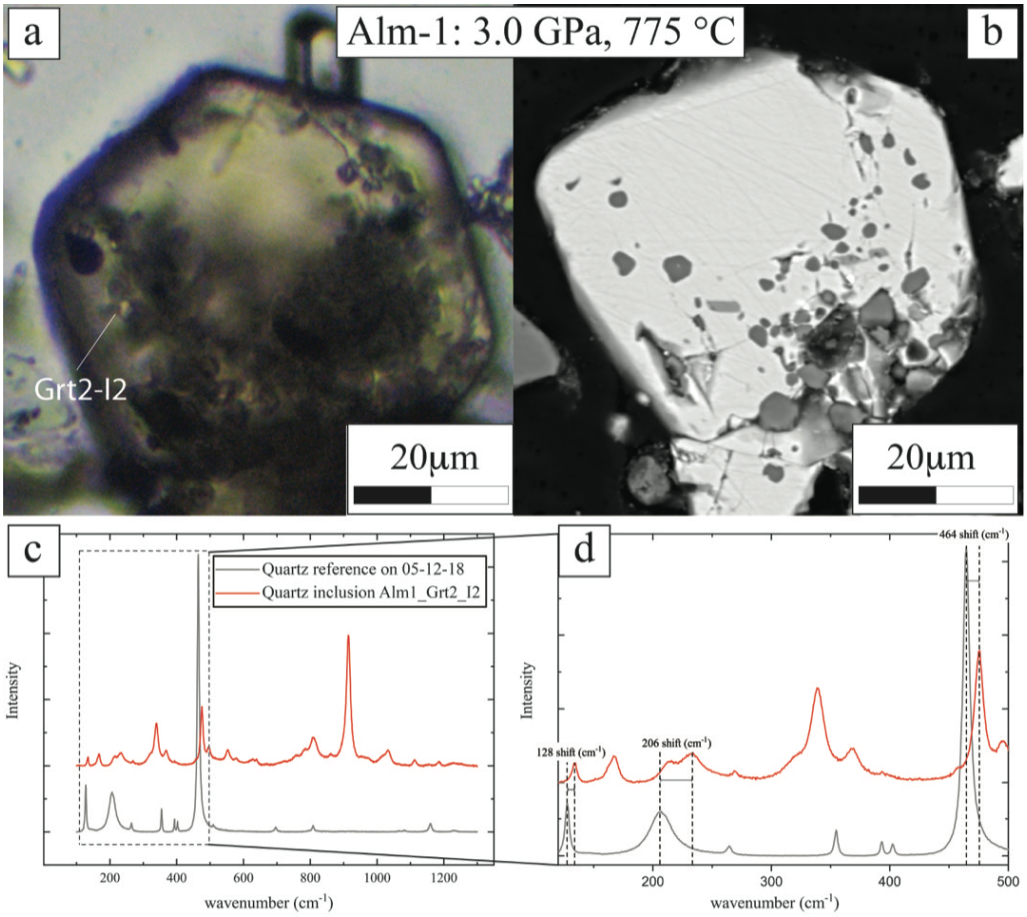

Fig. 2 - Optical microphotographs (a) and SEM-BSE images (b) of the sample Alm-1 that was synthesized at 3.0 GPa and 775°C (modified after Bonazzi *et al*., 2019). The garnet has euhedral shape with several trapped inclusions. An example of ideal inclusion is Grt2-I2. c) Raman spectrum of quartz reference and quartz inclusion Grt2-I2. d) Detail of the spectra for 128, 206 and 464 cm^{-1} Raman bands showing the shift of peak position of main Raman band between quartz reference and inclusion.

As starting materials, we used an oxide mix of SiO_2 (amorphous), Al_2O_3, FeO, Fe_2O_3 and TiO_2. In order to ensure that excess silica was present, the oxide mixture corresponded to the composition of almandine plus 24 wt.% excess silica. An equal weight of distilled water was added to completely wet the oxide mixture following the protocol of Thomas & Spear (2018), and approximately 10-15 mg of mixed oxides were loaded into silver capsules for each experiment. We used the design of Trail *et al.* (2012) in which the assembly was 12.7 mm in diameter and a silver capsule (~4 mm diameter) was formed by two identical parts separated by a platinum disk (150 µm thick) placed between the open ends of the half capsules (Fig. 1c). The oxygen fugacity was controlled using a double capsule technique in which one half-capsule contained the oxide mixture, and the other half contained an oxide mixture that crystallized fayalite, magnetite and quartz (see Fig. 1 in Thomas & Spear, 2018). We left headspace in both parts of the capsule for the addition of water and to avoid contaminating the tops of capsules with their contents. The cell assembly used in these experiments was the salt-pyrex-graphite with MgO filler. Temperature was measured with D-type thermocouples ($W_{97}Re_3$-$W_{75}Re_{25}$), situated within 1mm of the top of the capsule and was considered accurate to within ~10°C. The pressures in the piston-cylinder hydraulic rams were measured with Enerpac 140 MPa Bourdon-tube gauges with 18-cm-diameter dials. Experiments were cold pressurized to the desired run pressure followed by ramping the temperature at 100°C/minute. Runs were quenched to below 100°C in less than 60 s by turning off the furnace power. Pressure calibration of the piston cylinder was based on the quartz-coesite phase boundary (Boyd & England, 1960; Kitahara & Kennedy, 1964), using the same assemblies as our experiments.

Analytical methods

The inclusions were analyzed using Micro-Raman spectrometer and the spectra were acquired in backscattering geometry at 20°C and room pressure. As a standard, we used a band of silicon metal whose theoretical peak position is 520.7 cm^{-1}. The spot size was 1 μm and laser beam was focused on the center of inclusions because in that point the stress and strain of inclusions were not influenced by the shape. We measured several inclusions in several single garnet host and the measurement were repeated over several days to estimate their reproducibility. Overall, we collected data of at least 20 inclusions per experiment. The acquisition parameters were 5 acquisitions of 40 seconds each for inclusion. We fitted Raman spectra using a B-spline as a baseline correction and pseudo-Voigt peak functions with the OriginPro 2018b software. The estimated uncertainties on fitted peak positions were commonly < 0.3 cm. On the quartz included in the almandine we measured the wavenumber shifts of quartz inclusions relative to the line positions of a free quartz crystal at room temperature (see Fig. 2c and d).

Calculate entrapment pressure of quartz inclusions

The quartz crystal shows several vibration modes; however, for our quartz inclusions only the three most intense peaks (128, 206 and 464 cm^{-1}) were distinguishable from garnet (Fig. 2c). As shown in Figure 2d the wavenumber peaks position of free quartz and quartz inclusions (under residual pressure) had a shift. The residual pressure can be determined starting from wavenumber shifts of quartz Raman modes. For specific case of quartz inclusions in garnet the residual pressure (P_{inc}) can be calculated following two different approaches. The first method (*e.g.*, Enami *et al*., 2007; Ashley *et al.*, 2016; Thomas & Spear, 2018) considers that the quartz inclusions are under hydrostatic conditions. Then, the residual pressure of the inclusion was determined only from the wavenumber shifts at 464 cm^{-1}, by using the hydrostatic calibration of Schmidt & Ziemann (2000). However, this is an incorrect assumption for crystal trapped in other minerals, *e.g.*, when the quartz is incorporated in an almandine (cubic host) and the inclusion is subject to isotropic strains imposed by the host. Quartz has a deviatoric (*i.e.*, non-hydrostatic) stress because it is elastically anisotropic. For this reason, the wavenumber shifts of Raman band positions are correlated to the strain imposed by garnet host (*e.g.*, Grüneisen, 1926; Barron *et al.*, 1980; Cantrell Jr, 1980; Angel *et al.*, 2019). For this reason, different quartz crystals in the same garnet host exhibit different Raman shifts for the same Raman mode (*i.e.*, 464 cm^{-1}) because inclusions can be oriented in several way in the garnet host. The strains of quartz inclusions were related to Raman shift by using the phonon-mode Grüneisen tensors for quartz (Murri *et al.*, 2018; Angel *et al.*, 2019; Murri *et al*., 2019). At this point it was possible to use the strain components of quartz (ε_1 and ε_3) or Volume strain of quartz (V_S) to determine the residual stress. From strain components was necessary to use elastic tensor (Wang *et al.*, 2015) to calculate the stress components and the residual pressure (average of stresses) whereas for V_S was necessary to use the equation of state of the inclusion to determine the residual pressure.

From the residual pressures obtained with the different methods, it was possible to determine the entrapment pressures applying the equation of state by using The EosFit7 software suite (www.rossangel.net; Angel *et al*., 2014, 2017; Rosenfeld & Chase, 1961).

Results and discussions

We applied the previously described methods at the synthetic quartz inclusions to calculate the residual pressures (Fig. 3a and b).

The calculated P_{inc} from all measurements on the samples retrieved from both experiments were compared with the P_{inc} calculated from the known entrapment conditions from the isotropic host-inclusion model for spherical inclusions (Angel *et al*., 2014, 2017). As shown the Figures 3a and 3b, the residual pressure measured using the hydrostatic method ignores the effects of the elastic anisotropy of quartz (Bonazzi *et al.*, 2019). The discrepancy between the measured and the expected P_{inc} calculated for our synthesis conditions are larger for the experiment at 3 GPa and 775°C where the maximum discrepancy is about 0.7 GPa (Fig. 3a) than

for the experiment at 2.5 GPa (0.2 GPa; Fig. 3b). Therefore, it is reasonable that the anisotropy of quartz increases with increasing encapsulation pressures.

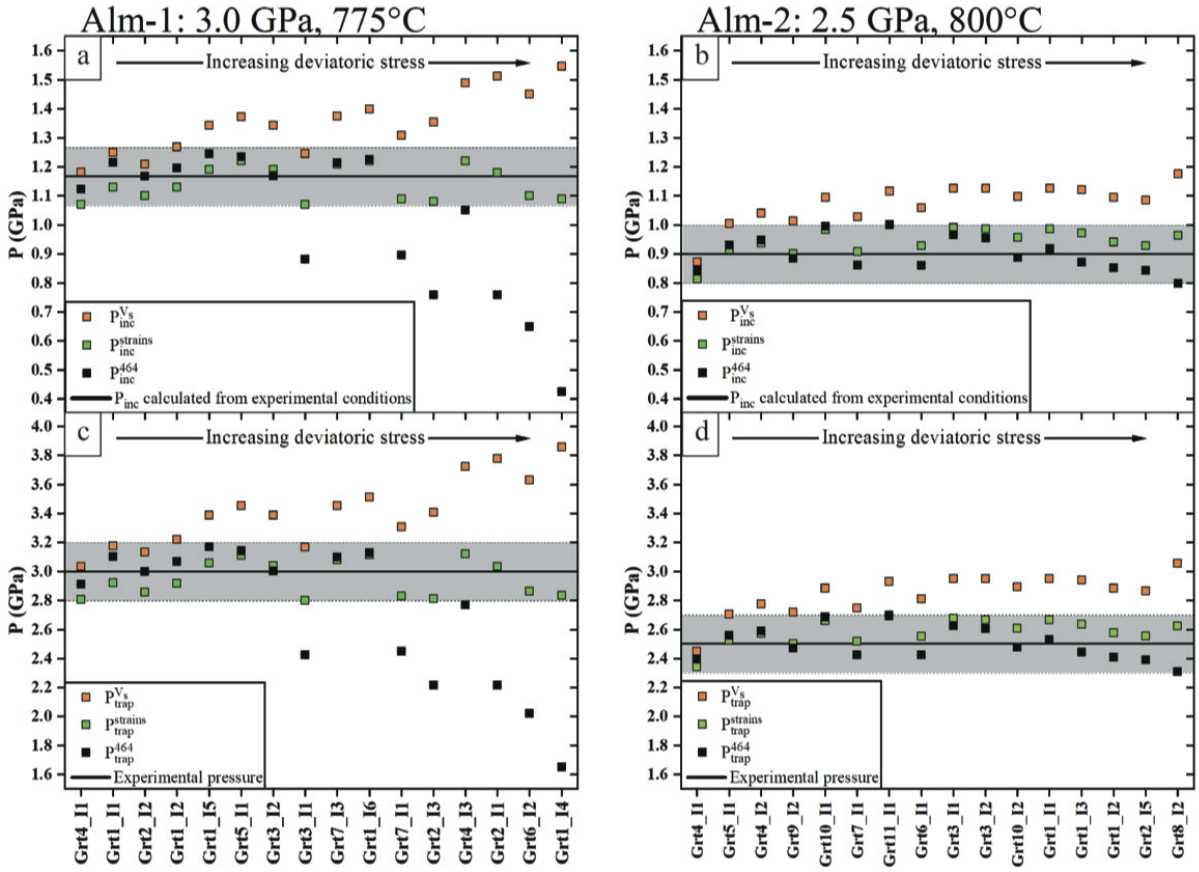

Fig. 3 - Residual pressures calculated for the quartz inclusions in garnet from synthesis at 3.0 GPa (a) and 2.5 GPa, (b). The black line represents the theoretical residual pressure (P_{inc}) for quartz in garnet calculated for the synthesis conditions. Entrapment pressures (P_{tra}) back-calculated by residual pressure for both methods of the synthesis at 3.0 GPa (c) and 2.5 GPa (d). The grey areas are the maximum uncertainties of the calculation. The squares indicate the P_{inc} and P_{trap} calculated from: 464 Raman shift using hydrostatic calibration (black), strain components using isotropic host inclusion model (green) and volume strain using isotropic host inclusion model (orange). Modified after Bonazzi *et al.* (2019).

Conversely, the residual inclusion pressure calculated from the V_s obtained by the hydrostatic EoS of quartz (Angel *et al.*, 2017) is generally overestimated than the theoretical P_{inc} (Fig. 3a and b). This effect occurs because the bulk modulus of quartz, decreases along the isochor from isostrain conditions (the Voigt bound on the bulk modulus) to hydrostatic conditions (the Reuss bound) and decrease until the ε_1 becomes more negative and ε_3 becomes more positive (Bonazzi *et al.*, 2019). For this reason, the hydrostatic bulk modulus (Reuss bound) overestimates the true residual inclusion pressure.

The P_{inc} calculated from mean stress $(2\sigma_1+\sigma_3)/3$ is obtained from strain components (ε_1 and ε_3) and the elastic tensor at room conditions of quartz (Wang *et al.*, 2015). The discrepancies of the measured and the theoretical P_{inc} are smaller than 0.1 GPa for both synthesis conditions (Fig. 3a and b). As shown for the high-P experiment (Fig. 3a), the deviation from the expected residual pressures using the strain method keeps constant for both experiments, whereas the errors in P_{inc} obtained by using the hydrostatic calibration of the 464 cm^{-1} line significantly increase at higher inclusion pressures.

From these residual pressures we calculated the entrapment pressures (P_{trap}) using the equations of state of the host and the inclusions (*e.g.*, Rosenfeld & Chase, 1961; Angel *et al.*, 2017) and we compared the calculated entrapment pressures with the known synthesis conditions. The results demonstrate that the effect of the anisotropy of quartz influence the accuracy of P_{trap}.

The P_{trap} calculated from the strain components are in good agreement with the experimental pressures of synthesis for both experiments. The obtained values from the volume strain (V_s) are too high compared to synthesis pressure for the reasons explained above. The entrapment pressures from V_s are more overestimated when the strains of quartz inclusions are far from hydrostatic conditions (Bonazzi *et al.*, 2019). On the contrary the hydrostatic calibration of the Raman shifts agrees with the synthesis pressure of the experiment at 2.5 GPa (Fig. 3d) but with the experiment at 3 GPa the discrepancy reaches up to 1.2 GPa (Fig. 3c). These discrepancies are related to the effects of quartz anisotropy at high pressures (Bonazzi *et al*., 2019).

CONCLUSIONS

In this work two methods to synthesize and validate the elastic geobarometry method for host-inclusion systems were developed. The solid-state syntheses results are still incomplete, but it has been produced quasi-ideal host-inclusion pairs that could be used to validate the elastic geobarometry approach using X-ray diffraction. These experiments have been extremely challenging as most of the protocols did not exist for these types of materials. Nonetheless, we had the opportunity to explore some growth and transformation processes occurring very rapidly at modest P and T. The growth process is basically suppressed by using crystalline powder with micrometric size. The process could certainly be improved significantly at higher temperature; nevertheless, the time to grow suitable sized grains would be too long to have significantly large single crystals. Therefore, we replaced the crystalline powder with more reactive non-crystalline powder, thus improving the quality of the host.

However, we reached an ideal host-inclusions pairs only with hydrothermal synthesis which allowed to synthesize quartz inclusions in garnet host (Fig. 1a). The inclusions were enough large, fully embedded, free of cracks and isolated in the garnet host to be measured. We could retrieve the synthesis pressures using Raman spectroscopy and applying elastic barometry on the ideal inclusions. Moreover, we determined the pressure on the inclusion using two different approaches (hydrostatic calibration and Grüneisen tensors) to assess the reliability of the results. The entrapment pressures calculated from the residual pressure obtained adopting the mode Grüneisen tensors approach was always more accurate than those calculated using the hydrostatic calibration. As shown in Fig. 3, it was demonstrated for the first time that the discrepancies between the results obtained with our protocol (*e.g.*, Murri *et al*., 2018; Bonazzi *et al*., 2019) and those obtained with previously proposed methods were mainly caused by wrong assumption regarding the elastic anisotropy of the pair. The most significant result of this study is that the elastic anisotropy of quartz influences the calculation of entrapment pressure (P_{trap}) of inclusions.

REFERENCES

Angel, R.J., Mazzucchelli, M.L., Alvaro, M., Nimis, P., Nestola, F. (2014): Geobarometry from host-inclusion systems: the role of elastic relaxation. *Am. Mineral*., **99**, 2146-2149.

Angel, R.J., Mazzucchelli, M.L., Alvaro, M., Nestola, F. (2017): EosFit-Pinc: A simple GUI for host-inclusion elastic thermobarometry. *Am. Mineral*., **102**, 1957-1960.

Angel, R.J., Murri, M., Mihailova, B., Alvaro, M. (2019): Stress, strain and Raman shifts. *Z. Krist-cryst Mater*., **234**, 129-140.

Ashley, K.T., Steele-MacInnis, M., Bodnar, R.J., Darling, R.S. (2016): Quartz-in-garnet inclusion barometry under fire: Reducing uncertainty from model estimates. *Geology*, **44**, 699-702.

Barron, T., Collins, J., White, G. (1980): Thermal expansion of solids at low temperatures. *Adv. Phys.*, **29**, 609-730.

Bonazzi, M., Tumiati, S., Thomas, J.B., Angel, R.J., Alvaro, M. (2019): Assessment of the reliability of elastic geobarometry with quartz inclusions. *Lithos*, **350**, 105-201.

Boyd, F. & England, J. (1960): Apparatus for phase-equilibrium measurements at pressures up to 50 kilobars and temperatures up to 1750°C. *J. Geophys. Res*., **65**, 741-748.

Cantrell Jr, J.H. (1980): Generalized Grüneisen tensor from solid nonlinearity parameters. *Phys. Rev. B*, **21**, 41-91.

Chopin, C. (1984): Coesite and pure pyrope in high-grade blueschists of the Western Alps: a first record and some consequences. *Contrib. Mineral. Petr.*, **86**, 107-118.

Compagnoni, R. & Hirajima, T. (2001): Superzoned garnets in the coesite-bearing Brossasco-Isasca Unit, Dora-Maira massif, Western Alps, and the origin of the whiteschists. *Lithos*, **57**, 219-236.

Enami, M., Nishiyama, T., Mouri, T. (2007): Laser Raman microspectrometry of metamorphic quartz: A simple method for comparison of metamorphic pressures. *Am. Mineral.*, **92**, 1303-1315.

Grüneisen, E. (1926): Zustand des festen Körpers. *In*: "Thermische Eigenschaften der Stoffe", C. Drucker *et al*., eds. Springer, Berlin, Heidelberg, 1-59.

Howell, D., Wood, I.G., Nestola, F., Nimis, P., Nasdala, L. (2012). Inclusions under remnant pressure in diamond: a multi-technique approach. *Eur. J. Mineral*., **24**, 563-573.

Ikesue, A. & Aung, Y.L. (2006): Synthesis and performance of advanced ceramic lasers. *J. Am. Ceram. Soc.*, **89**, 1936-1944.

Izraeli, E., Harris, J., Navon, O. (1999): Raman barometry of diamond formation. *Earth Planet. Sc. Lett.*, **173**, 351-360.

Kitahara, S. & Kennedy, G. (1964): The quartz-coesite transition. *J. Geophys. Res.*, **69**, 5395-5400.

Murri, M., Mazzucchelli, M.L., Campomenosi, N., Korsakov, A.V., Prencipe, M., Mihailova, B., Scambelluri, M., Angel R.J., Alvaro, M. (2018): Raman elastic geobarometry for anisotropic mineral inclusions. *Am. Mineral.*, **103**, 1869-1872.

Murri, M., Alvaro, M., Angel, R.J., Prencipe, M., Mihailova, B. (2019): The effects of non-hydrostatic stress on the structure and properties of alpha-quartz. *Phys. Chem. Miner*., **46**, 487-499.

Nestola, F., Nimis, P., Ziberna, L., Longo, M., Marzoli, A., Harris, J.W., Manghnani, M.H., Fedortchouk, Y. (2011): First crystal-structure determination of olivine in diamond: Composition and implications for provenance in the Earth's mantle. *Earth Planet. Sc. Lett.*, **305**, 249-255.

Rezende, M.V.D.S. (2014): Pressure dependence of dielectric constant, elastic constants, and lattice parameters of the $Y_3(Ga,Al)_5O_{12}$ host. *J. Phys. Chem. Solids*, **75**, 1113-1118.

Rosenfeld, J.L. & Chase, A.B. (1961): Pressure and temperature of crystallization from elastic effects around solid inclusions in minerals? *Am. J. Sci*., **259**, 519-541.

Schmidt, C. & Ziemann, M.A. (2000): In-situ Raman spectroscopy of quartz: A pressure sensor for hydrothermal diamond-anvil cell experiments at elevated temperatures. *Am. Mineral.*, **85**, 1725-1734.

Simon, G., Chopin, C., Schenk, V. (1997): Near-end-member magnesiochloritoid in prograde-zoned pyrope, Dora-Maira massif, western Alps. *Lithos*, **41**, 37-57.

Thomas, J.B. & Spear, F.S. (2018): Experimental study of quartz inclusions in garnet at pressures up to 3.0 GPa: evaluating validity of the quartz-in-garnet inclusion elastic thermobarometer. *Contrib. Mineral. Petr.*, **173**, 42.

Tingle, T.N. (1988): Retrieval of uncracked single crystals from high pressure in piston-cylinder apparatus. *Am. Mineral*. **73**, 1195-1197.

Trail, D., Watson, E.B., Tailby, N.D. (2012): Ce and Eu anomalies in zircon as proxies for the oxidation state of magmas. *Geochim. Cosmochim. Ac*., **97**, 70-87.

Wang, J., Mao, Z., Jiang, F., Duffy, T.S. (2015): Elasticity of single crystal quartz to 10 GPa. *Phys. Chem. Miner*., **42**, 203-212.